ELSEVIER

Cement & Concrete Composites 22 (2000) 343–351

Cement & Concrete Composites

www.elsevier.com/locate/cemconcomp

Fracture properties of concrete reinforced with steel–polypropylene hybrid fibres

Chunxiang Qian [a,*], Piet Stroeven [b]

[a] Department of Materials Science and Engineering, Southeast University, Nanjing 210096, People's Republic of China
[b] Faculty of Civil Engineering and Geosciences, Delft University of Technology, Delft, The Netherlands

Received 30 April 1999; accepted 25 May 2000

Abstract

This research discusses polypropylene fibres and three sizes of steel fibres reinforced concrete. The total fibre content ranges from 0% to 0.95% by volume of concrete. A four-point bending test is adopted on the notched prisms with the size of $100 \times 100 \times 500$ mm^3 to investigate the effect of hybrid fibres on crack arresting. The research results show that there is a positive synergy effect between large steel fibres and polypropylene fibres on the load-bearing capacity and fracture toughness in the small displacement range. But this synergy effect disappears in the large displacement range. The large and strong steel fibre is better than soft polypropylene fibre and small steel fibre in the aspect of energy absorption capacity in the large displacement range. The static service limitation for the hybrid fibres concrete, with "a wide peak" or "multi-peaks" load–CMOD patterns, should be carefully selected. The ultimate load bearing capacity and the crack width or CMOD at this load level should be jointly considered in this case. The K_{IC} and fracture toughness of proper hybrid fibre system can be higher than that of mono-fibre system.

Keywords: Polypropylene fibre; Steel fibre; Fracture properties; Low fibre content

1. Introduction

The function of short-cut fibres as secondary reinforcement in concrete is mainly to inhibit crack initiation and propagation. The basic purpose in using hybrid fibres is to control cracks at different size levels, in different zones of concrete (cement paste or interface zone between paste and aggregate), at different curing ages and at different loading stages. The large and the strong fibres control large cracks. The small and soft fibres control crack initiation and propagation of small cracks. This research focuses on the polypropylene (PP)–steel hybrid fibres reinforced system. Mono-filament PP fibre and three sizes of steel fibres will be discussed.

2. Materials

1. Cement used is Portland type C from ENCI Maastricht of the Netherlands. Its sieve residue of 45 μm is 3.22%. The characteristic strength is 52.5 MPa.
2. A low-lime type of fly ash was applied. It was from Cementbouw Mineralen, B.V. The physical characteristics are listed in Table 1. Density was tested according to Dutch recommendation NEN3550. Loss on ignition and moisture content were measured according to ASTM C311. Sieve residue of 45 μm was tested according to ASTM C430.
3. PP fibre was from A.B.G. Bouw-en Handelsonderneming B.V. of the Netherlands. The fibre type is mono-filament with a length of 12 mm and a diameter of 18 μm.
4. Steel fibres were from Bekaert in Belgium. Three types of steel fibres were used in this research. SF1 type is hooked, with a length of 40 mm and a diameter of about 0.3 mm. SF2 type is also hooked, with a length of 30 mm and a diameter about 0.3 mm. SF3 type is plain, with a length of 6 mm and a diameter of less than 0.1 mm.
5. The superplasticizer (SP) used in this research was from DESMEPOL B.V. of the Netherlands. It is on a melamine basis with solid content of 35%. Its maximum dosage is 3.0% by weight of the cement.
6. The aggregate gradation adopted in this research is shown in Table 2.

* Corresponding author. Tel.: +86-25-379-4392; fax: +86-25-771-2719.
E-mail address: cxqian@publicl.ptt.js.cn (C. Qian).

0958-9465/00/$ - see front matter
PII: S0958-9465(00)00033-0

Table 1
Physical characteristics of fly ash

Density	Loss on ignition	45 μm Sieve residue	Moisture content
2.248 (g/cm^3)	3.63 (%)	14.92 (%)	0.11 (%)

3. Experimental program

3.1. Design of experiments

A series of seven factors and two levels of a factorial design are used in this research on the basis of our previous research [1,2]. All specimens used 400 kg/m^3 of cement, 100 kg/m^3 of fly ash and a water–cement ratio of 0.40. The fibre contents by volume of concrete for each batch of specimens are listed in Table 3. C1–C8 belong to the factorial design. C9, plain concrete, and C10, mono-fibre concrete are used as references.

3.2. Specimens making and curing

The mixing procedure is the same as employed for the reference mixtures [1,2]. For each batch of concrete, seven cubes of 150 mm and one slab sized 500 mm × 400 mm×100 mm were made. Three cubes were used for compressive strength testing after curing for 28 days at 23 ± 3°C and 95–100% RH. Three cubes were used for splitting strength testing. One cube was used for the analysis of fibre distribution. The slab was sawn into 3 prisms of 100 mm × 100 mm × 500 mm after curing one month at 23 ± 3°C and 95–100% RH. Before the bending test, the prisms were provided with a central notch with a depth of 30 mm and a width of 3 mm. Table-vibrating time of fresh concrete is 36 s for the casting of the cubes and 24 s for the slabs.

3.3. Splitting test

The splitting plane is the vertical central section of the cube. The cube is turned over 90° with respect to casting direction.

3.4. Four-point bending test

The test set-up and the arrangement of displacement sensors (LVDT) are shown in Figs. 1(a)–(e). The displacement at the initial notch tip, recorded by LVDT13 in Fig. 1(b), was used as feedback signal to control the loading process. The displacement rate is 0.5 μm/s before the displacement reaches 1 mm. After this value, the rate increases about three times. The load and the displacements are recorded by personal computer during the whole loading process. The displacements from LVDT11, LVDT12, LVDT21, LVDT22, corresponding to the two loading points, are indicated by D11, D12, D21 and D22, respectively, in the following discussion. LVDT2m is located near the centre of the specimen and its displacement is indicated by D2m. The displacement from LVDT13, located at the initial notch tip, is indicated by CTOD. The signal from LVDTb expresses the crack mouth opening displacement that is indicated by CMOD. The signal from LVDTt indicates by Dt. It reflects the deformation due to compression at the top of the specimens.

Table 2
Aggregate gradations (taking 0.125–16 mm particles as 100%)

Size (mm)	0.125–0.250	0.250–0.5	0.5–1	1–2	2–4	4–8	8–16	0.125–4
Weight (%)	3	11	11	10	10	25	30	45.0

Table 3
Fibres content for each batch of specimens

Group no.	PP (%)	SF1 (%)	SF3 (%)	SF2 (%)	Total (%)
C1	0	0.2	0.2	0	0.4
C2	0	0.2	0.4	0	0.6
C3	0	0.4	0.2	0	0.6
C4	0	0.4	0.4	0	0.8
C5	0.15	0.2	0.2	0	0.55
C6	0.15	0.2	0.4	0	0.75
C7	0.15	0.4	0.2	0	0.75
C8	0.15	0.4	0.4	0	0.95
C9	0	0	0	0	0
C10	0	0	0	0.6	0.6

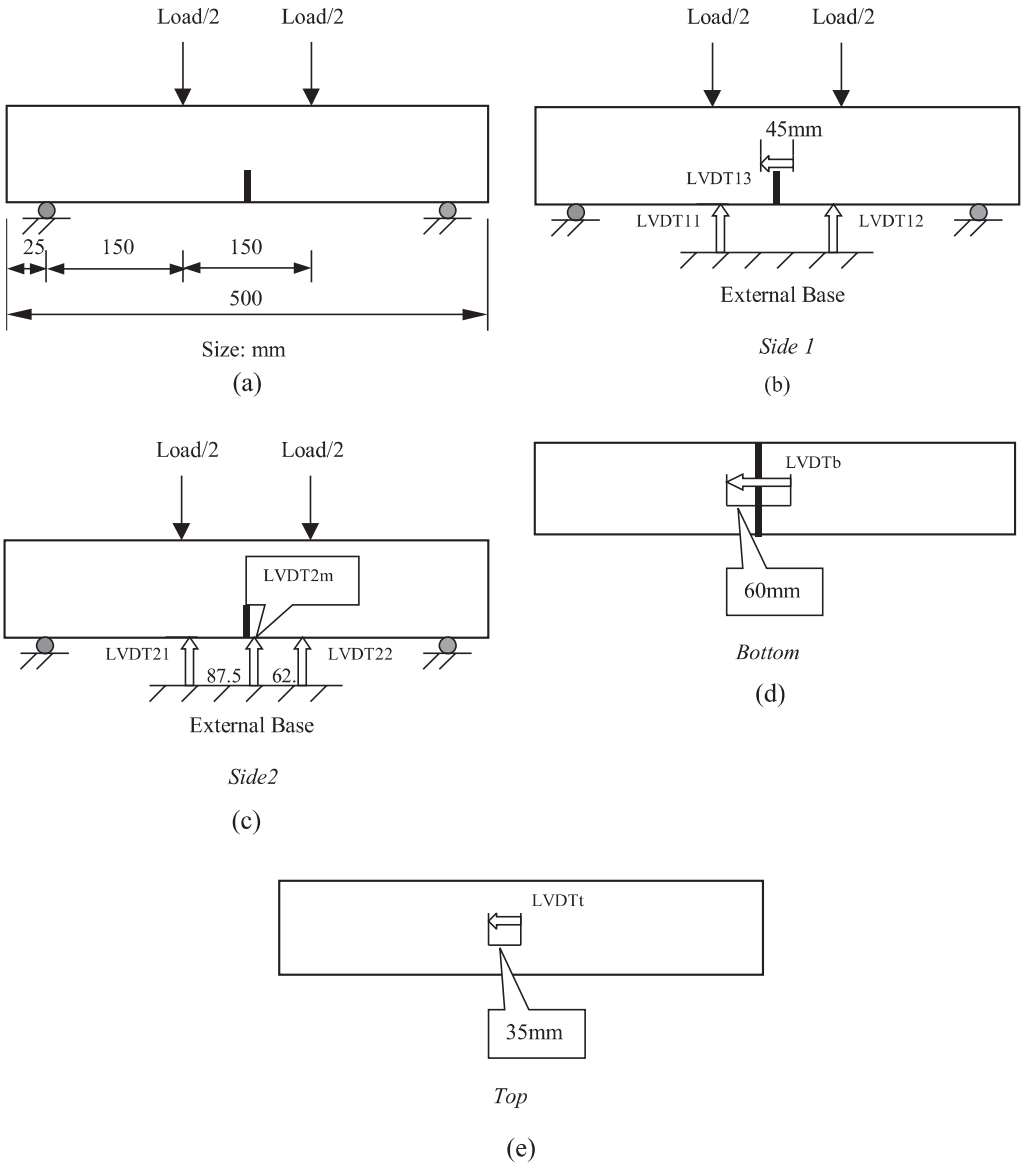

Fig. 1. Four-point bending test set-up and arrangement of displacement sensors.

4. Experimental results

4.1. General properties of concrete

The unit weight, the slump of the fresh concrete, the compressive (f_c) and the splitting strengths (f_{spl}) at 28 days are listed in Table 4. The content of SP varies somewhat to control the workability of fresh concrete. The contents are all by weight of the cement. The value between brackets is the in-group coefficient of variation.

4.2. Pattern of load–displacement graphs

Figs. 2 and 3 show the load–CMOD patterns of hybrid fibre concretes, of mono-fibre concrete C10 and of plain concrete C9. The curves represent in-group averages of loads at the same displacement. It can be seen that the patterns of hybrid fibre concretes are different from those of plain concrete and mono-fibre concrete both in the pre- and the post-ultimate range.

4.3. Characteristics in pre-ultimate load region

The loads at CMOD values of 50 μm (L_5) and 100 μm (L_1) and the ultimate load (L_p) are used to evaluate the properties of hybrid fibre concretes in the pre-ultimate region. These parameters jointly represent the load-bearing characteristics under service conditions. These parameters for hybrid fibre concretes investigated in this research are listed in Table 5. The

Table 4
General properties of concrete

Group no.	Unit weight (kg/m^3)	Slump (mm)	f_c (MPa)	f_{spl} (MPa)	SP (%)
C1	2418 (0.4%)	160	72.7 (0.6%)	4.97 (5.7%)	2.5
C2	2422 (0.4%)	140	76.0 (0.6%)	5.29 (3.7%)	2.5
C3	2431 (0.4%)	110	76.0 (1.2%)	5.37 (10.8%)	2.5
C4	2436 (0.4%)	140	76.6 (3.9%)	5.78 (8.2%)	2.6
C5	2399 (0.3%)	100	74.4 (4.3%)	5.58 (5.4%)	3.0
C6	2410 (0.2%)	75	71.2 (6.2%)	5.98 (3.2%)	3.0
C7	2407 (0.5%)	40	72.8 (2.0%)	6.11 (5.0%)	3.0
C8	2410 (0.4%)	30	73.7 (3.3%)	6.53 (5.4%)	3.0
C9	2389 (0.4%)	150	68.0 (0.6%)	4.34 (2.5%)	2.0
C10	2441 (0.6%)	200	80.8 (2.0%)	6.77 (1.9%)	2.5

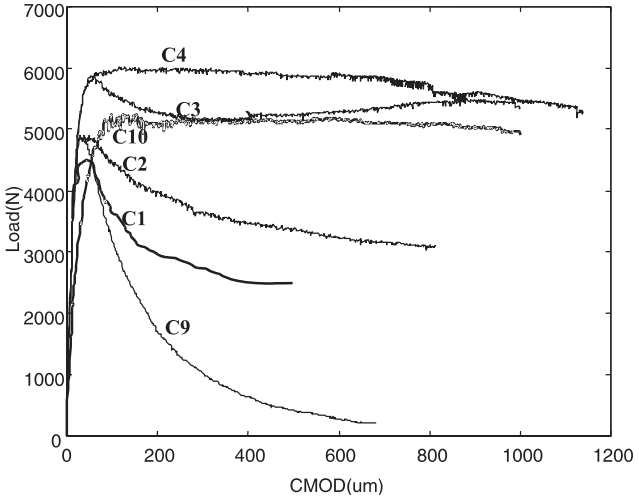

Fig. 2. Load–CMOD curve pattern.

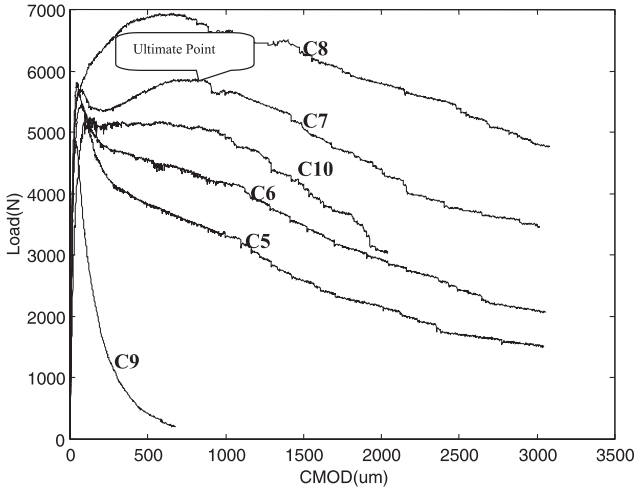

Fig. 3. Load–CMOD curve pattern.

ultimate load here means the maximum load on the whole load–CMOD curve as shown in Fig. 3.

In Table 5, the value between the brackets gives the in-group coefficient of variation. $CMOD_p$ is CMOD at the ultimate load point on the load–CMOD curve.

The normal service limitation for hybrid fibres concrete should be made out on the basis of two aspects: load bearing capacity (the ultimate load) and the value of CMOD. CMOD is related to crack width. For example, in some circumstances durability requirements would lead to a crack width limit of up to 100 μm. The ultimate load for plain concrete C9 and the low-performance hybrid fibre concrete C1 and C2 should be used as serviceability limits. The load at a certain limiting value of CMOD, such as L_1 should be used as a serviceability limit for high-performance hybrid fibre concrete, revealing multi-peaks or a wide peak in the load–CMOD curve. For example, the crack width for C3, C4, C7 and C8 should be used as the serviceability limit even though they have high load bearing capacity even after large displacements such as 100 μm. So, the serviceability limit at normal state for hybrid fibre concretes and normal plain concrete will be different. The high performance hybrid fibres concrete will give obvious information (large CMOD) before it reaches its ultimate load in the case of unexpected over-load, i.e., it reveals high ductility.

4.4. Correlation of various displacements

The displacements of D11, D12, D21, D22 and D2m measured according to Fig. 1 contain two parts. The major part is due to pure bending of the prisms, on which this research is focusing. The second part is caused by non-plane-parallelism of the bottom surface of the prism leading to parasitic deformations due to torsion. Those two parts can be easily separated in the experimental graphs, furthermore, the real deflections can be found out. There are linear relationships between various deflections and CMOD. Table 6 presents the

Table 5
Characteristics of hybrid fibre concretes in pre-ultimate region

Group	L_5 (N)	L_1 (N)	L_p (N)	$CMOD_p$ (μm)
C1	4730, 5020, 4200	3910, 3850, 3600	4740, 5150, 4590	48, 60, 32
Average	4650 (8.9%)	3787 (4.3%)	4827 (6.0%)	
C2	4450, 4520, 5670	3920, 3890, 5570	4560, 4680, 5760	60, 31, 62
Average	4880 (14%)	4460 (22%)	5000 (13.2%)	
C3	5480, 5680, 6360	5160, 5460, 6150	5520, 6090, 6510	46, 879, 71
Average	5840 (7.9%)	5590 (9.1%)	6040 (8.2%)	
C4	5390, 5670, 6250	5740, 5410, 6610	5890, 5720, 6920	314, 60, 375
Average	5570 (7.6%)	5920 (10%)	6177 (10.5%)	
C5	5790, 5520, 5940	5140, 5190, 5610	5910, 5690, 6010	56, 42, 46
Average	5743 (3.6%)	5313 (4.8%)	5870 (2.8%)	
C6	5730, 4650, 6030	5670, 4320, 5510	5850, 4730, 6160	70, 56, 45
Average	5470 (13.3%)	5167 (14.3%)	5580 (13.5%)	
C7	5370, 6330, 5750	5070, 6120, 5390	5620, 7740, 5840	1000, 841, 64
Average	5817 (8.3%)	5527 (9.7%)	6400 (18.2%)	
C8	5650, 5450, 5700	6400, 5660, 5830	8080, 5740, 7510	770, 108, 660
Average	5600 (2.4%)	5963 (6.5%)	7110 (17.2%)	
C9	5130, 4260, 4470	3610, 3010, 3010	5250, 5000, 4530	40, 28, 34
Average	4620 (9.8%)	3210 (10.8%)	4927 (7.4%)	
C10	4630, 5310, 4520	5220, 5750, 4720	5740, 5850, 4990	645, 86, 225
Average	4820 (8.9%)	5230 (9.8%)	5527 (8.5%)	

Table 6
Values of the slope of the displacements versus CMOD relationships

Group	D11	D12	D21	D22	D2m	CTOD	Dt
C1	0.4248 (6%)	0.5111 (4%)	0.5065 (1%)	0.5360 (16%)	0.7289 (11%)	0.9249 (2%)	−0.2296 (6%)
C2	0.4553 (1%)	0.5247 (8%)	0.4823 (14%)	0.4092 (15%)	0.5935 (12%)	0.9047 (2%)	−0.1630 (15%)
C3	0.4797 (20%)	0.5137 (9%)	0.4891 (10%)	0.4856 (2%)	0.6850 (2%)	0.8578 (6%)	−0.1940 (27%)
C4	0.4200 (9%)	0.5675 (8%)	0.5068 (6%)	0.6000 (10%)	0.7830 (10%)	0.9076 (3%)	−0.1823 (22%)
C5	0.4229 (6%)	0.4853 (6%)	0.4512 (4%)	0.4860 (4%)	0.6559 (6%)	0.9276 (1%)	−0.1613 (4%)
C6	0.4189 (5%)	0.4923 (3%)	0.4800 (6%)	0.4998 (3%)	0.6617 (4%)	0.9213 (1%)	−0.1724 (5%)
C7	0.4451 (9%)	0.4662 (8%)	0.4994 (8%)	0.4783 (3%)	0.6703 (5%)	0.8993 (4%)	−0.1519 (14%)
C8	0.4639 (3%)	0.4601 (4%)	0.4516 (7%)	0.4797 (5%)	0.6796 (4%)	0.8918 (3%)	−0.1843 (9%)
C9	0.4429 (10%)	0.3944 (18%)	0.4876 (17%)	0.4417 (6%)	0.6606 (6%)	0.9393 (2%)	−0.1884 (3%)
C10	0.4308 (3%)	0.4780 (4%)	0.4589 (7%)	0.4647 (15%)	0.6565 (13%)	0.8739 (2%)	−0.1579 (28%)
Average	0.4404 (9%)	0.4892 (11%)	0.4811 (8%)	0.4881 (13%)	0.6775 (10%)	0.9043 (3%)	−0.1785 (18%)

value of the slope of these linear relationships. It is shown that the differences between the different groups are statistically insignificant. There are following general equations:

$$\mathrm{Dt} = -0.1785(\mathrm{CMOD}), \tag{1}$$

$$\mathrm{D2m} = 0.6775(\mathrm{CMOD}), \tag{2}$$

$$\mathrm{CTOD} = 0.9043(\mathrm{CMOD}), \tag{3}$$

$$(\mathrm{D11}, \mathrm{D12}, \mathrm{D21 \text{ or } D22}) = 0.4747(\mathrm{CMOD}). \tag{4}$$

4.5. Critical stress intensity factor K_{IC}

According to Brown and Strawley [3], K_{IC} for pure bending of cement-based materials can be written as

$$K_{IC} = [6M_c/b(w-a)^2](\pi a)^{1/2} Y(a/w), \tag{5}$$

$$Y(a/w) = (1/\pi)^{1/2}(1-a/w)^2[1.99 - 2.47(a/w)] + 12.97(a/w)^2 - 23.17(a/w)^3 + 24.80(a/w)^4, \tag{6}$$

where M_c is the critical moment, b the beam width, w the beam depth, a the notch depth and $Y(a/w)$ is a polynominal.

The K_{IC} calculated from experimental ultimate loads in Table 5 are listed in Table 7.

4.6. Fracture toughness

Several methods have been proposed to evaluate the fracture toughness of cement-based materials [4–9], for example, ASTM C1018 (four-point bending), RILEM 50-FMC Draft Recommendation (three-point bending with notched beam), Japan Institution of Standard (four-point bending), Canadian post-crack strengths etc. This paper adopts the method similar to JCI method and Canadian post-crack strength. JCI method uses the area of load-mid span deflection curve of four-point bending as evaluation parameter while mid span deflection is equal to span/150. The deflection tested in this research was only upon to 2 mm. So, the deflection of span/225 (2 mm), span/450 (1 mm) and span/1350 (0.5 mm) are used to evaluate the fracture toughness of fibre concrete. The results are listed in Table 7.

The post-crack strength for four-point bending proposed by Banthia [7] can be written as

$$\mathrm{PCS} = [A_{\mathrm{post}}L]/[(D - D_p)bw^2], \tag{7}$$

where D_p is the deflection at peak load. For multi-peak curve, D_p is the deflection of first peak. A_{post} is the area of load–deflection curve after peak load or first peak load as shown in Fig. 4. In this research, PCS for notched beam can be written as

$$\mathrm{PCS} = [A_{\mathrm{post}}L]/[(D - D_p)b(w - a)^2]. \tag{8}$$

The results are listed in Table 7.

5. Discussions

5.1. Influence of fibre type and size on properties

In this research, the properties of hybrid fibre concrete are evaluated by means of L_5, L_1, L_p, K_{IC} and post-crack strength. The statistical analysis results are listed in Table 8.

The influences of various factors on the properties are as follows:

L_5: SF1 > PP ≈ PP*SF1,
L_1: SF1 > PP ≈ PP*SF1 > SF3,
L_p/K_{IC}: SF1 > PP,
PCS at deflection of 0.5 mm ($PCS_{0.5}$): SF1 > PP = SF3 > SF1*PP,
PCS at deflection of 2 mm (PCS_2): SF1 > SF3.

The effects of the other factors are not significant on the indicated parameters.

There are positive synergy effects between SF1 and PP (SF1*PP) on load bearing capacities (L_5, L_1) and fracture toughness ($PCS_{0.5}$) at small displacement stages. This synergy effect disappears at the large displacement stages (L_p, K_{IC}, PCS_2). Even though the ratio of length over diameter of SF3 is as high as 600, its effect is not as good as SF1. Because SF3 is plain, SF1 is hooked.

5.2. Comparison between hybrid fibre concrete and mono-fibre concrete

Fig. 5 illustrates the comparison between mono-fibre concrete C10 and hybrid fibre concretes C2, C3 and C5. They included different types and sizes of fibres but with the similar volume content of fibres. The K_{IC}, PCS at deflection of 0.5 mm ($PCS_{0.5}$) and PCS at deflection of 2 mm (PCS_2) of hybrid fibre system C3 are higher than that of mono-fibre system C10. The K_{IC} of hybrid system C5 is higher than that of mono-fibre system C10. It

Table 7
Critical stress intensity factor and fracture toughness of hybrid fibre concrete

	K_{IC}, MN/m$^{3/2}$	JCI Method (N m)			PCS (MPa)		
		$D = L/1350$	$D = L/450$	$D = L/225$	$D = L/1350$	$D = L/450$	$D = L/225$
C1	23.68	1.06	3.04	5.67	2.83	2.71	2.55
C2	24.54	1.30	4.06	7.96	3.53	3.67	3.59
C3	29.66	1.74	5.38	9.96	4.82	4.90	4.51
C4	30.33	1.95	6.59	11.78	5.45	6.02	5.35
C5	28.90	1.48	3.69	5.68	4.02	3.31	2.53
C6	27.38	1.60	4.39	7.13	4.41	3.96	3.20
C7	31.40	1.82	5.62	9.80	5.04	5.12	4.43
C8	34.91	2.11	6.61	12.26	5.94	6.04	5.57
C9	24.19	0.60	0.60	0.60	1.37	0.43	0.20
C10	27.13	1.69	4.84	7.29	4.73	4.41	3.31

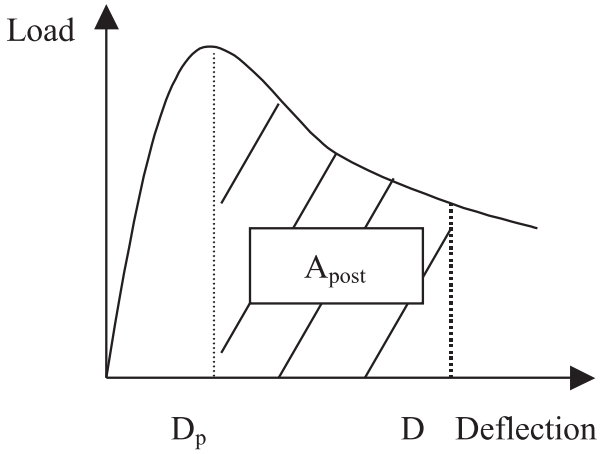

Fig. 4. Illustration of A_{post}.

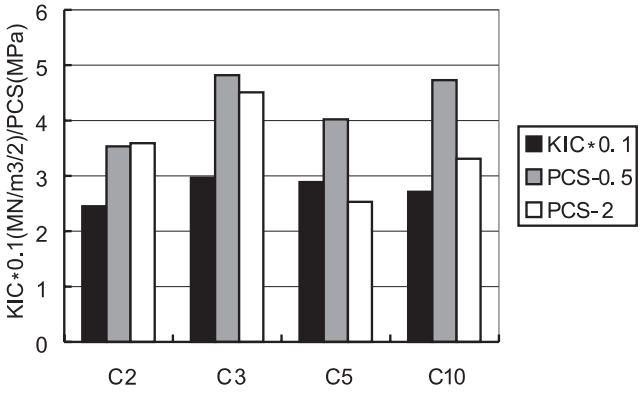

Fig. 5. Comparison between mono-fibre concrete and hybrid fibre concrete C2: 0.2% SF1 + 0.4 SF3% (total: 0.6%); C3: 0.4% SF1 + 0.2% SF3 (total: 0.6%). C5: 0.15% PP + 0.2% SF1 + 0.2% SF3 (total: 0.55%); C10: 0.60% SF2.

means that the proper hybrid fibre system can be more efficient than mono-fibre system.

5.3. Influence of PP on K_{IC} and fracture toughness

It can be seen from Fig. 6 that PP fibre obviously improves the K_{IC} by comparison between C1 and C5, C2 and C6, C3 and C7, C4 and C8. This conclusion agrees well with above statistical analysis. From Fig. 7, it can be seen that PP improves JCI fracture toughness to a certain extent at the deflection of L/1350(0.5 mm) and L/450(1 mm). But PP almost does not improve JCI toughness except C8 at the deflection of L/225 (2 mm). Fig. 8 shows further information about the effect of PP. PP does not improve PCS at large deflection stage (2 mm). But at small deflection stage (0.5 mm), PP increases the PCS by comparison of C1–C5, C2–C6, C3–C7 and C4–C8. The improvement degree of PCS decreases with the increase of total fibre content by comparison of (C1–C5, C2–C6) and (C3–C7, C4–C8). This is because high fibre content will affect the dispersion of PP.

Table 8
Factorial design and results

Group		PP	SF1	PP*SF1	SF3	PP*SF3	SF1*SF3	Scatter	L_5	L_1	L_p	$PCS_{0.5}$	PCS_2
C1		1	1	1	1	1	1	1	4650	3787	4827	2.83	2.55
C2		1	1	1	2	2	2	2	4880	4460	5000	2.53	3.59
C3		1	2	2	1	1	2	2	5840	5590	6040	4.82	4.51
C4		1	2	2	2	2	1	1	5570	5920	6177	5.45	5.35
C5		2	1	2	1	2	1	2	5743	5313	5870	4.02	2.53
C6		2	1	2	2	1	2	1	5470	5167	5580	4.41	3.20
C7		2	2	1	1	2	2	1	5817	5527	6400	5.04	4.43
C8		2	2	1	2	1	1	2	5600	5963	7110	5.49	5.57
L_5	K_1	5235	5186	5214	5512	5390	5391	5377					
	K_2	5658	5707	5656	5380	5502	5502	5516	L_5, L_1, L_p: MPa				
	R	423	521	442	−132	112	111	139	K_1: sum of first level				
L_1	K_1	4939	4682	4934	5054	5127	5246	5100	K_2: sum of second level				
	K_2	5492	5750	5498	5378	5305	5186	5532	R: difference of K_2 and K_1				
	R	554	1068	558	324	178	−60	232	PP*SF1: interaction between PP and SF1				
L_p	K_1	5511	5319	5834	5784	5889	5996	5746	PP*SF3: interaction of PP and SF3				
	K_2	6240	6432	5917	5967	5862	5755	6005	SF1*SF3: interaction of SF1 and SF3				
	R	729	1113	83	183	−27	−241	259	Scatter: influence of experimental scatter				
$PCS_{0.5}$	K_1	4.16	3.70	4.33	4.18	4.50	4.43	4.43					
	K_2	4.85	5.31	4.68	4.83	4.51	4.45	4.58					
	R	0.69	1.61	0.34	0.65	0.01	0.02	0.15					
PCS_2	K_1	4.00	2.97	4.04	3.50	3.96	4.00	3.88					
	K_2	3.93	4.96	3.90	4.43	3.98	3.93	4.05					
	R	−0.07	2.00	−0.14	0.93	0.02	−0.07	0.17					

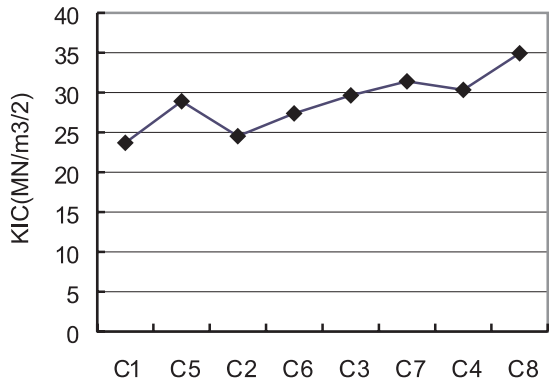

Fig. 6. Influence of PP fibre on K_{IC}.

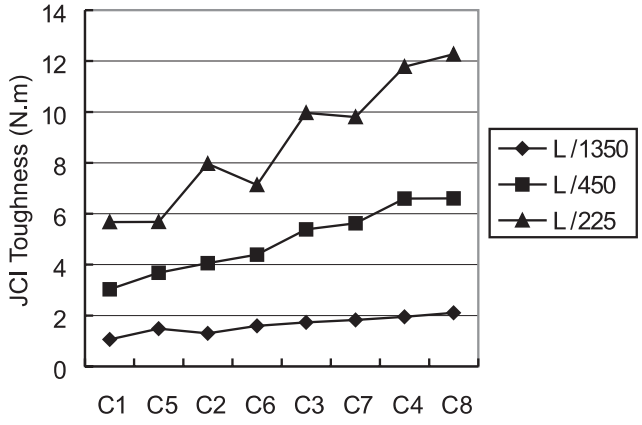

Fig. 7. Influence of fibre addition on fracture toughness by JCI method.

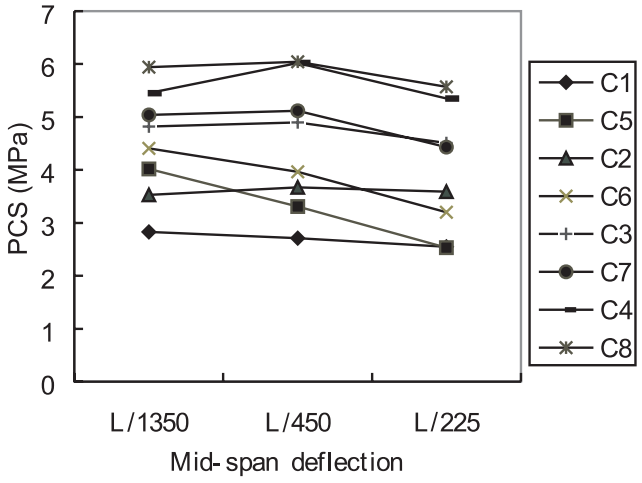

Fig. 8. Influence of PP on fracture toughness by PCS.

6. Conclusions

On the basis of four-point bending tests on notched prisms and the statistical analysis, the following conclusions can be drawn:

- The large steel fibres SF1 and the PP fibre significantly influence the load bearing capacity of hybrid fibres concrete in the small displacement range. Herein, the small plain steel fibres SF3 also exert a certain effect.
- The steel fibres SF1 affect most significantly on the energy absorption capacity in the large displacement range. In this respect, the effect of SF3 is more obvious than PP.
- There is a positive synergy effect between SF1 and PP on the load-bearing capacity and fracture toughness in the small displacement range. But this synergy effect disappears in the large displacement range.
- The effect of PP at small deflection stage decreases with the increase of total fibres content because of the dispersion of PP fibres.
- Among three types of steel fibres SF1, SF2 and SF3, SF1 is the best one. Because it is hooked compared to plain SF3 and it is with high length–diameter ratio compared to SF2.
- The relations between various displacements and CMOD tested in this research are as follows. They correspond to the specimen sizes and the experimental set-up used in this research:

$$\mathrm{Dt} = -0.1785(\mathrm{CMOD}),$$
$$\mathrm{D2m} = 0.6775(\mathrm{CMOD}),$$
$$\mathrm{CTOD} = 0.9043(\mathrm{CMOD}),$$
$$(\mathrm{D11}, \mathrm{D12}, \mathrm{D21 \text{ or } D22}) = 0.4747(\mathrm{CMOD}).$$

Acknowledgements

The authors gratefully acknowledge the financial support by Royal Dutch Academy of Science and the support from Ministry of Science and Technology of China. The authors would also like to give thanks to CICAT of TU Delft for its non-technical support and the support from Foreign Affair Office and Personnel Affair Office, Southeast University, China, particularly Prof. Sun Wei. This research obtained technical support from following people: Mr. Leen Donker, Ir. Peng Xiang, Ing. D.H. Dalhuisen, Ing. Paul Vermeulen, Ing. C. van Beek, Mr. F.J.L. Custers. The authors gratefully acknowledge their work.

References

[1] Qian C, Stroeven P. Optimization of hybrid polypropylene–steel fibres reinforced concrete. Technical Report 03.21.1.32.13, 1998.
[2] Qian C, Stroeven P. Properties of concrete reinforced with polypropylene–steel hybrid fibres. Technical Report 03.21.1.32.14, 1998.
[3] Ziegeldorf S. Fracture mechanics parameters of hardened cement paste, aggregates and interfaces. In: Wittman FH, editor. Fracture Mechanics of Concrete. Amsterdam: Elsevier, 1983. p. 371–409.

[4] 50-FMC Draft recommendation, determination of the fracture energy of mortar and concrete by means of three-point bend tests on notched beams. Mater Struct 1985;18(106): 287–90.
[5] Hillerborg A. The theoretical basis of a method to determine the fracture energy G_f of concrete. Mater Struct 1985;18(106): 291–6.
[6] Gopalaratnam VS, Gettu R. On the characterization of flexural toughness in FRC. Cem Concr Compos 1995;17:48–57.
[7] Banthia N, Jean-Francois T. Test methods for flxural toughness characterization of fibre reinforced concrete: some concerns and proposition. ACI Mater J 1985;92(1):48–57.
[8] Shah SP, Swartz SE, Ouyang C. Fracture mechanics of concrete. New York: Wiley, 1995.
[9] Soroushian P, Elyamany H, Tlili A, Ostowari K. Mixed-mode fracture properties of concrete reinforced with low volume fractions of steel and polypropylene fibres. Cem Concr Compos 1998;20:67–78.